

## Model Hamiltonian Description of Ag-Au Alloys in the Coherent-Potential Approximation\*

K. Levin<sup>†</sup> and H. Ehrenreich

*Division of Engineering and Applied Physics, Harvard University, Cambridge, Massachusetts 02138*  
(Received 18 January 1971)

A simple model Hamiltonian relevant to binary noble-metal alloys is introduced. The model, which is easily treated in the coherent-potential approximation (CPA), contains one  $s$  band of finite width and one  $d$  level of zero width which hybridizes with the  $s$  band. The Hamiltonian is examined using the CPA in two ways: first, purely as a model whose properties can be simply investigated, and second, as a Hamiltonian which may be considered to approximate that appropriate to noble-metal alloys. In regard to the first aspect of the model, interest is centered on special limiting cases such as the dilute-alloy and split- $d$ -band limits. It is shown as a result of  $s$ - $d$  hybridization that the criterion for the split- $d$ -band limit in the two-band model is considerably more severe than in a one-band model investigated previously. In regard to the second aspect, interest is focused on some electronic properties of Au-Ag alloys. It is not expected that Wigner-Seitz cells within these alloys will be neutral. In order to explain the observed concentration dependence of the optical-absorption edge, it is necessary to assume that electrons are transferred from Au to Ag sites, rather than from Ag to Au as has been commonly supposed. The concentration dependence of the  $d$ -level positions is obtained from a "renormalized atom" theory and the charge transfer, which is assumed to arise from  $s$  electrons. The optical-absorption edge as a function of concentration is estimated from parameters appropriate to Ag-Au. Good qualitative agreement with experiment is obtained when the transfer of  $s$  electrons from Au to Ag atoms is taken into account. By contrast, the predicted behavior is qualitatively incorrect if charge-transfer effects are neglected or assumed to go in the opposite direction.

### I. INTRODUCTION

As is generally known, noble- and transition-metal band structures may be characterized by narrow tight-binding  $d$  bands which hybridize with a broad  $s$ - $p$  conduction band. In the present paper a new one-electron model is introduced which contains some but not all of these essential features of noble and transition metals and their binary alloys  $A_x B_{1-x}$ . The pure crystals  $A$  and  $B$  are assumed to contain one  $s$  band of finite width and one  $d$  band of zero width at energy  $\epsilon_d^{A,B}$  which hybridizes with the  $s$  band; thus the structure of the  $d$  bands is neglected here. In the alloy Hamiltonian  $H^{\text{alloy}}$  the  $d$  resonance energy at a given site  $\epsilon_d^n$  may take on one of two  $x$ -dependent values corresponding to whether an  $A$  or  $B$  atom is at site  $n$ . The unhybridized  $s$  bands and the hybridization constants are treated in the virtual-crystal approximation. By contrast, the  $d$  bands, whose potentials are not expected to be weak, are treated in the coherent-potential approximation (CPA).<sup>1,2</sup> Using the CPA, approximate configuration-averaged densities of states may be determined for alloys of arbitrary concentration and reasonably strong scattering strengths.  $H^{\text{alloy}}$  is examined using the CPA in two ways: first, purely as a model whose properties can be simply investigated, and second, as a Hamiltonian which may be considered to approximate that appropriate to noble-metal alloys.

In regard to the first aspect of the model, inter-

est is centered on special limiting cases, such as the dilute-alloy and split- $d$ -band limits. It is shown that as a result of  $s$ - $d$  hybridization, the criterion for the split- $d$ -band limit in the two-band model is considerably more severe than in the one-band model investigated previously.<sup>1</sup> In regard to the second aspect, interest is focused on the first strong optical interband transition in Au-Ag alloys. It is not expected that Wigner-Seitz cells within these alloys will be neutral. Arguments are presented which indicate that  $s$  electrons are transferred from one alloy component to the other. On the basis of present band calculations<sup>3</sup> and interband optical data,<sup>4,5</sup> it seems reasonable to conclude that this charge transfer is from Au to Ag sites, rather than from Ag to Au as has been commonly assumed.<sup>6,7</sup> This view seems to be the only one consistent with the observed behavior of the optical-absorption edge as a function of alloy concentration.

The most serious objection to this point of view arises from isomer-shift data. The analysis of these data, while careful and detailed, is nevertheless based on some assumptions whose validity we are not prepared to question in the absence of further calculations. The contradiction is hopefully more apparent than real. Optical and Mössbauer data, respectively, sample the regions outside and inside the core. The charge density in these regions may vary differently with concentration.

A renormalized atom theory<sup>8</sup> is used to calculate

the  $x$  dependence of  $\epsilon_d^{Au,Ag}(x)$  which arises from  $s$ -electron transfer in the alloy; it is seen that the position of the  $d$  levels is concentration dependent as a result of the concentration dependence of the  $s$  charge transferred. The  $x$  dependence of the optical-absorption edge obtained from the Hamiltonian is in good qualitative agreement with experiment<sup>4,5</sup> when the parameters appropriate to Au-Ag are properly chosen.

Previous theories with one exception which have attempted to describe the electronic properties of Au-Ag have either considered only the dilute-alloy limit<sup>9</sup> or have treated the alloy scattering strength perturbatively<sup>10</sup>: Recently, a more general calculation of the electronic properties of Au-Ag in the one-band CPA has been performed in an analysis of photoemission data. Charge-transfer effects were not considered, however.<sup>11</sup> Calculations of dilute-alloy properties have neglected the  $d$  electron entirely.<sup>9</sup> The  $s$  electrons were assumed to scatter in a square well whose depth, computed self-consistently, was determined by the difference in energy between the bottom of the  $s$  band of the host and that of the impurity.<sup>9</sup> In calculations of non-dilute alloys the total scattering potential was assumed to be weak and the wave functions computed perturbatively.<sup>10</sup> In the dilute-alloy calculations it was found using a Thomas-Fermi picture that a net  $s$  charge was deposited on the atom with the most attractive potential. On the basis of an entirely different picture,<sup>10</sup> it was inferred from the dependence of the optical-absorption edge on impurity concentration that the  $d$  wave functions near the top of the band had greater amplitude on Au than Ag sites. This difference in wave-function amplitude was called "charging."<sup>10</sup>

An outline of the paper will now be given.<sup>12</sup> In Sec. IIA the model Hamiltonian  $H^{alloy}$  relevant to binary noble-metal alloys  $A_x B_{1-x}$  is characterized and the results of the CPA applied to  $H^{alloy}$  are outlined. The pure-metal limit ( $x=0$ , or  $x=1$ ) of  $H^{alloy}$  is discussed first and compared with the Hamiltonian commonly used in interpolation schemes.<sup>13,14</sup> Next, the results of the CPA applied to  $H^{alloy}$  are presented and three special limiting cases are considered in detail: the dilute-alloy limit (Sec. IIB), the atomic limit (Sec. IIC), and the split- $d$ -band limit (Sec. IID).

The purpose of Sec. III is to develop a model for  $Au_x Ag_{1-x}$  alloys based on  $H^{alloy}$ . In Sec. IIIA some relevant electronic properties of the pure metals Au and Ag are discussed. A renormalized atom theory<sup>3</sup> and a brief summary of the results of recent band calculations for Au and Ag will be described.<sup>3</sup> The Au-Ag alloy system is considered in Sec. IIIB. Both experimental and theoretical evidence for the lack of neutrality of Wigner-Seitz cells in these alloys is given. The evidence suggests that  $s$  elec-

trons are transferred from Au to Ag atoms in these alloys. In Sec. IIIC the Au-Ag alloy parameters, e.g.,  $\epsilon_d^{Au,Ag}(x)$ , are computed using the results of band calculations and the renormalized atom theory. An estimate of the  $s$  charge transfer in the dilute-alloy limits is given using the Thomas-Fermi model. The  $x$  dependence of the charge transfer for nondilute alloys is computed by linear interpolation between these limits. This last assumption has some experimental basis which will be discussed. The  $x$  dependence of the  $s$  charge transferred is then used to calculate the  $x$  dependence of the positions of the  $d$  levels  $\epsilon_d^{Au,Ag}(x)$ .

In Sec. IV the results found in Secs. II and III are numerically illustrated. The  $s$  and  $d$  densities of states and other quantities for pure Au and Ag and for several alloy concentrations are discussed in Sec. IVA. The latter calculations are performed for a value of the charge-transfer parameter  $\Delta Q^{Ag}(x \approx 1) = 0.3e$ . This parameter is defined to be the  $s$  charge transferred to a single Ag atom in an Au host. Arguments are presented to show that noble-metal alloys are *not* in a split- $d$ -band limit.<sup>15</sup> Two artificial alloys will be discussed to illustrate this limit. In Sec. IVB a calculation of the concentration dependence of the first interband optical-absorption edge in  $Au_x Ag_{1-x}$  alloys is presented. Experimental results<sup>4,5</sup> are discussed first and these are compared with theory for four different values of the charge-transfer parameter  $\Delta Q^{Ag}(x \approx 1) = 0.3e, -0.2e, +0.5e, 0$ . It is seen that the best agreement with experiment is obtained for  $\Delta Q^{Ag}(x \approx 1) = 0.3e$  in accord with estimates made in Sec. III. Very poor agreement is obtained if the charge-transfer effects are neglected or if  $s$  electrons are transferred from the Ag to the Au atoms instead of from the Au to the Ag.

## II. CHARACTERIZATION OF MODEL HAMILTONIANS AND APPLICATION OF CPA

### A. Description of Model: Application of CPA

In this section a new one-electron model alloy Hamiltonian  $H^{alloy}$  is introduced and its properties investigated. In some respects this may be regarded as appropriate to binary noble-metal alloys. It is convenient to begin by considering the pure-crystal limit of  $H^{alloy}$  to be denoted  $H^{Metal}$ ,

$$H^{Metal} = \sum_{\vec{k} \in BZ} |\vec{k}_s\rangle \epsilon_s(\vec{k}) \langle \vec{k}_s| + \sum_n |n_d\rangle \epsilon_d \langle n_d| + \sum_{\vec{k} \in BZ} [\gamma(\epsilon_d) |\vec{k}_s\rangle \langle \vec{k}_d| + \gamma(\epsilon_d) |\vec{k}_d\rangle \langle \vec{k}_s|] \quad (2.1)$$

The crystal is assumed to have only one  $s$  and one  $d$  band. The energy origin is  $\Gamma_1$ , the bottom of the unhybridized  $s$  band. The latter has a width  $2w_s$ , determined by the intersection of the unhybridized  $s$ -band energy-wave-number dispersion relation

$\epsilon_s(\vec{k})$  and the Brillouin-zone boundary.  $\epsilon_d$  represents the position of the  $d$  resonance measured relative to  $\Gamma_1$ ; the  $\gamma$  characterizes the strength of the  $s$ - and  $d$ -electron hybridization and depends only on  $\epsilon_d$  as is indicated;  $n$  is a site index. The hybridization width of the  $d$  level is to be associated with the width of the  $d$  band; spin and orbital degeneracies are explicitly absent in (2.1). These effects are included schematically by assuming the  $d$  level has ten  $d$  electrons and the  $s$  band is filled by two electrons per atom.

In the pure crystal  $\vec{k}$  is a good quantum number and thus mixing can only take place between  $s$  and  $d$  electrons with the same  $\vec{k}$  eigenvalue. Equation (2.1) should be contrasted with the Anderson Hamiltonian (in the absence of Coulomb interactions) with a single  $d$  resonant level at site 0 in a free-electron band<sup>16</sup>:

$$H^A = \sum_{\vec{k}} |\vec{k}_s\rangle \langle k_s^2/2m | \vec{k}_s | + |0_d\rangle \epsilon_d \langle 0_d| + \sum_{\vec{k}} (V_{kd} |\vec{k}_s\rangle \langle 0_d| + \text{c. c.}) . \quad (2.2)$$

Here mixing takes place between the  $d$  electrons at the impurity site and the free electrons from the host; thus  $\vec{k}$  is not a good quantum number. In  $H^A$  the hybridization constant  $V_{kd}$  is considered to be  $k$  dependent, but for ease in computation it is usually approximated by a constant.

The model Hamiltonian of (2.1) is a simplified version of that used by other investigators<sup>17,18</sup> to fit the electron band structure of Cu, and later formally derived by Heine<sup>13</sup> and also by Hubbard.<sup>14</sup> Comparing Eq. (2.1) with the Heine-Hubbard Hamiltonian<sup>13,14</sup> it is seen that the term represented by  $\epsilon_s(\vec{k})$  in (2.1) is replaced in Heine's formalism by a matrix containing four orthogonalized plane waves  $K$ . As a consequence of transforming away higher-order plane waves, the  $d$  levels become effectively broadened, so that the term diagonal in  $|n_d\rangle$  space and independent of  $k$  in Eq. (2.1) is replaced by a  $k$ -dependent matrix  $D_{mm}$  in Ref. 13. Also, in the formalism of Ref. 13, the hybridization constants  $\gamma_{km}$  are shown to depend both on  $k+K$  and with whichever of the five tight-binding orbitals, denoted by  $m$ , the  $s$  electrons are hybridizing. The gross simplifications present in the model Hamiltonian [Eq. (2.1)] are therefore evident.

It is shown in Ref. 13 that for  $k$  along symmetry directions  $\Gamma L$  and  $\Gamma X$  in the Brillouin zone, only one of the  $d$  bands hybridizes with the plane-wave band due to symmetry. These consist of  $d$  states with  $m=0$  quantized about the direction of  $k$  as axis. Evaluating  $\gamma_{k0}$  at  $k = \sqrt{\epsilon_d}$ , it follows that  $\gamma_{\sqrt{\epsilon_d}0} = M' \epsilon_d$ . The constant of proportionality  $M'$  is seen to be about 0.3 for Cu and for the rest of the 3d-transition series.<sup>13</sup> When considering noble metals, it will be assumed here that  $\gamma$  in (2.1) is given by  $\gamma_{\sqrt{\epsilon_d}0}$  with  $M'=0.3$ . This approximation, although

serious for Au and Ag, is no more so than the neglect of structure of the  $d$  bands. This choice of  $\gamma$  is not unreasonable for the applications to optical properties to be considered in the present paper when other constants such as  $E_F - \Gamma_1$  are chosen appropriately.

Some insight into the properties of the model Hamiltonian (2.1) can be gained by calculating the energy vs wave-number dispersion relation  $E(\vec{k})$  for the two hybridized bands. The secular equation for  $H^{\text{Metal}}$  and its solution are, respectively,

$$[\epsilon_s(\vec{k}) - E(\vec{k})][\epsilon_d - E(\vec{k})] - \gamma^2 = 0 \quad (2.3)$$

and

$$E_{\pm}(k) = \frac{1}{2} \{ \epsilon_d + \epsilon_s(k) \pm [ (\epsilon_d - \epsilon_s(k))^2 + 4\gamma^2 ]^{1/2} \} . \quad (2.4)$$

Here it is assumed for simplicity that  $\epsilon_s(\vec{k})$  is isotropic in  $k$ ,<sup>19</sup> i. e. ,

$$\epsilon_s(\vec{k}) = \epsilon_s(k) . \quad (2.5)$$

As shown in Fig. 1(a),  $\epsilon_s(k)$  is bounded above and below by  $\epsilon_s(k^{\text{max}}) \equiv \epsilon^{\text{max}}$  and  $\epsilon_s(k^{\text{min}}) \equiv \epsilon^{\text{min}}$  determined, respectively, by the Brillouin-zone boundary and center. Thus

$$\epsilon_d \geq E_-(k^{\text{max}}) \geq E_-(k) \quad (2.6)$$

and

$$\epsilon_d \leq E_+(k^{\text{min}}) \leq E_+(k) . \quad (2.7)$$

The behavior of  $E_+$  and  $E_-$  as functions of  $k$  for the parameters of Fig. 1(a) is sketched in Fig. 1(b). Equations (2.6) and (2.7) indicate that for crystals with isotropic  $\epsilon_s(k)$  there will be an energy gap in the density of states which contains the resonance energy  $\epsilon_d$ , provided all higher bands are neglected. The gap width is determined by  $|E_+(k^{\text{min}}) - E_-(k^{\text{max}})|$ . It should be emphasized that in actual noble metals, this gap in the density of states is clearly absent since there are five  $d$  bands of finite width with which the  $s$  electrons may hybridize.

The discussion here will treat Eq. (2.1) in two ways: first, as a model whose properties can be simply investigated, and second, as a Hamiltonian which may be considered to approximate that appropriate to noble metals. It is in this second context that spurious features such as a gap in the density of states must be reconciled with physical reality. The applications of Eq. (2.1) to noble metals and its extension to the alloy case will not be concerned with the structural details of the  $d$  or  $s$  bands. Attention will be focused primarily on the position of the top of the  $d$  band relative to the Fermi energy, the  $d$  bandwidth, and the width of the  $s$  band. In these considerations the gap is an unessential property of the model Hamiltonian.

We shall assume that in a noble-metal alloy  $A_x B_{1-x}$  the Hamiltonian is given by

$$H^{\text{alloy}} = \sum_{\vec{k} \in \text{BZ}} |\vec{k}_s\rangle \epsilon_s(\vec{k}) \langle \vec{k}_s | + \sum_n |n_d\rangle \epsilon_d^n(x) \langle n_d |$$

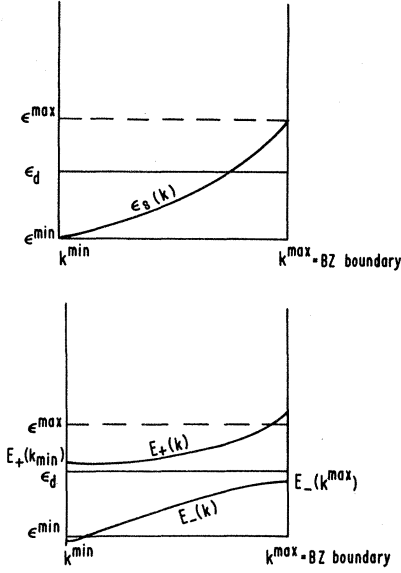


FIG. 1. Energy vs wave number  $k$  for hybridized bands: (a) unhybridized  $E$  vs  $k$  relation; (b) hybridized  $E$  vs  $k$  for one dimension in  $k$  space.

$$+ \sum_{\vec{k} \in \text{BZ}} [\gamma(\bar{\epsilon}_d) |\vec{k}_s\rangle \langle \vec{k}_d| + \gamma(\bar{\epsilon}_d) |\vec{k}_d\rangle \langle \vec{k}_s|]. \quad (2.8)$$

Here the parameter  $\epsilon_d^n(x)$  can take on one of two values, depending on whether an A or a B atom is at site  $n$ . In contrast to previous work,<sup>1</sup> we shall consider the possibility that  $\epsilon_d^n$  is concentration dependent and that its value may be determined in some consistent fashion. In the limit  $x \rightarrow 0$ ,  $\epsilon_d^n(x) \rightarrow \epsilon_d^B$  and similarly as  $y \equiv 1 - x \rightarrow 0$ ,  $\epsilon_d^n(x) \rightarrow \epsilon_d^A$ , where  $\epsilon_d^{A,B}$  characterizes the position of the  $d$  resonance level in the pure A or B crystals measured relative to the appropriate  $\Gamma_1$ . In this section the argument  $x$  will not be explicitly indicated.

We assume that the kinetic energy term involving  $\epsilon_s(k)$  is the same as in the pure crystal. In addition, it seems reasonable to treat the position of the bottom of the  $s$  band  $\bar{\Gamma}_1$  in the virtual-crystal approximation in which

$$\bar{\Gamma}_1 = x\Gamma_1^A + y\Gamma_1^B. \quad (2.9)$$

Similarly in the alloy  $\gamma(\bar{\epsilon}_d) \equiv \bar{\gamma}$  is evaluated at the average  $d$  resonance energy  $\bar{\epsilon}_d = x\epsilon_d^A + y\epsilon_d^B$ . It is therefore concentration dependent. The only random term appearing in  $H^{\text{alloy}}$  is the term which describes the unhybridized  $d$  band.

The CPA<sup>1,2</sup> may be easily applied to (2.8). We may define a self-energy operator  $\hat{\Sigma}_d(z) = [\Sigma_d(z)]\hat{P}_d$ , where  $\hat{P}_d$  is a projection operator onto the space of  $d$  states, in terms of the configuration-averaged propagator  $\bar{G}_k$  (diagonal in the crystal Bloch basis) by

$$\langle (z - H^{\text{alloy}})^{-1} \rangle_k \equiv \bar{G}_k = \begin{pmatrix} z - \epsilon_s(k) & -\bar{\gamma} \\ -\bar{\gamma} & z - \Sigma_d \end{pmatrix}^{-1}. \quad (2.10)$$

The brackets  $\langle \dots \rangle$  denote a configuration average. Here we have written  $\bar{G}_k$  as a  $2 \times 2$  matrix corresponding to the basis vectors  $\{|k_s\rangle, |k_d\rangle\}$ . The unaveraged propagator for the electrons in the alloy  $G = (z - H^{\text{alloy}})^{-1}$  may be expressed in terms of  $\bar{G}$  by defining a scattering operator  $T$  using

$$G = \bar{G} + \bar{G}T\bar{G}. \quad (2.11)$$

Because of the assumed localization of  $d$  states, the random term in Eq. (2.8) is a sum of single-site contributions. Hence multiple-scattering theory may be used to write

$$T = \sum_n T_n + \sum_{n \neq m} T_n \bar{G} T_m + \dots, \quad (2.12)$$

where

$$T_n = V_n(1 + \bar{G}T_n) \quad (2.13)$$

is the scattering matrix associated with the site  $n$ , and the effective scattering potential is

$$V_n = \begin{pmatrix} 0 & 0 \\ 0 & \epsilon_d^n - \Sigma_d \end{pmatrix} \quad (2.14)$$

in the basis  $\{|n_s\rangle, |n_d\rangle\}$ . Equation (2.13) may be written in this basis as

$$T_n = \begin{pmatrix} 0 & 0 \\ 0 & T_n^{dd} \end{pmatrix}. \quad (2.15)$$

Here

$$T_n^{dd} = (\epsilon_d^n - \Sigma_d)[1 - (\epsilon_d^n - \Sigma_d)F_{dd}(z, \Sigma_d)]^{-1} \quad (2.16)$$

and

$$\begin{aligned} F_{dd}(z, \Sigma_d) &= N^{-1} \text{Tr}_d \bar{G}(z) \\ &= N^{-1} \sum_{k \in \text{BZ}} \langle k_d | \bar{G} | k_d \rangle = \langle n_d = 0 | \bar{G}(z) | n_d = 0 \rangle. \end{aligned} \quad (2.18)$$

The relation  $\text{Tr}_d$  indicates the trace over  $d$  states, only, and  $|k_d\rangle$  is the Bloch transform of the Wannier  $d$  ket  $|n_d\rangle$ .

The CPA applied to (2.12), together with the definition of  $\bar{G}$  as the averaged propagator, implies that

$$\langle T_n^{dd} \rangle = 0. \quad (2.19)$$

This leads to the usual  $k$ -independent equation for the self-energy<sup>1,2</sup>:

$$\Sigma_d(z) = \bar{\epsilon}_d - [\epsilon_d^A - \Sigma_d(z)]F_{dd}(z, \Sigma_d)[\epsilon_d^B - \Sigma_d(z)], \quad (2.20)$$

where

$$\bar{\epsilon}_d = x\epsilon_d^A + y\epsilon_d^B \quad (2.21)$$

Equation (2.17) may also be written

$$\begin{aligned} F_{dd}(z, \Sigma_d) &= \Omega_c (2\pi)^{-3} \int_{\text{BZ}} d^3 \vec{k} \\ &\times \{z - \Sigma_d - \bar{\gamma}^2 [z - \epsilon_s(\vec{k})]^{-1}\}^{-1}, \end{aligned} \quad (2.22)$$

the  $\Omega_c$  being the unit-cell volume. This equation can be simplified by defining

$$\rho_{0s}(E) = \Omega_c (2\pi)^{-3} \int_{\text{BZ}} d^3\vec{k} \delta(E - \epsilon(\vec{k})), \quad (2.23)$$

where  $\rho_{0s}(E)$  is the density of states (per site) in the unhybridized  $s$  band normalized to 1. It follows from (2.22) that

$$F_{dd}(z, \Sigma_d) = (z - \Sigma_d)^{-1} + \bar{\gamma}^2 (z - \Sigma_d)^{-2} F_{0s}[z - \bar{\gamma}^2 (z - \Sigma_d)^{-1}], \quad (2.24)$$

where

$$F_{0s}(z) = \int_{-\infty}^{\infty} \rho_{0s}(E) (z - E)^{-1} dE. \quad (2.25)$$

Despite its appearance, Eq. (2.24) has no singularity at  $z = \Sigma_d$ . This may be seen by observing that since the spectrum is bounded as  $z \rightarrow \Sigma_d$ ,

$$F_{0s}[z - \bar{\gamma}^2 (z - \Sigma_d)^{-1}] \rightarrow - (z - \Sigma_d) (\bar{\gamma})^{-2}.$$

Consequently, the two singular terms in  $F_{dd}(z, \Sigma_d)$  cancel.

The average density of states per site in the alloy can be computed from  $\bar{G}$ . Since there are ten  $d$  electrons per atom, the average density of  $d$  states per atom is

$$\begin{aligned} \rho_d(E, \Sigma_d) &= -10(N\pi)^{-1} \text{ImTr}_d \bar{G}(E + i0) \\ &= -10(N\pi)^{-1} \text{Im} \sum_{k \in \text{BZ}} \langle k_d | \bar{G} | k_d \rangle \\ &= -10\pi^{-1} \text{Im} \langle n_d = 0 | \bar{G}(E + i0) | n_d = 0 \rangle, \end{aligned} \quad (2.26)$$

where in this last equation it is assumed that  $\bar{G}$  is the operator whose matrix representation is given by (2.10). From (2.17) it follows that

$$\rho_d(E, \Sigma_d) = -10\pi^{-1} \text{Im} F_{dd}(E + i0, \Sigma_d^+). \quad (2.27)$$

Similarly, the density of states for  $s$  electrons is

$$\rho_s(E, \Sigma_d) = -2(N\pi)^{-1} \text{ImTr}_s \bar{G}(E + i0) \quad (2.28)$$

$$= -2\pi^{-1} \text{Im} F_{ss}(E + i0, \Sigma_d^+), \quad (2.29)$$

where in analogy with (2.17) and (2.22)

$$F_{ss}(z, \Sigma_d) = N^{-1} \text{Tr}_s \bar{G}(z) \quad (2.30)$$

$$= F_{0s}[z - \bar{\gamma}^2 (z - \Sigma_d)^{-1}]. \quad (2.31)$$

In Eq. (2.30),  $\text{Tr}_s$  is understood to mean that the trace is to be taken over the subspace of  $s$  states. We will frequently write quantities such as  $F_{ss}(z, \Sigma_d)$  as  $F_{ss}(z)$ .

$F_{ss}(z)$  and  $F_{dd}(z)$  are both analytic everywhere in the complex  $z$  plane except for branch cuts on the real axis. The discontinuity of  $F_{dd}$  across the real axis is given by

$$F_{dd}(E + i0) - F_{dd}(E - i0) = 2i \text{Im} F_{dd}(E^*). \quad (2.32)$$

A similar equation may be written for  $F_{ss}$ . Since  $F_{0s}(z) \sim z^{-1}$  as  $z \rightarrow \infty$ , it follows from (2.24) that  $F_{dd}(z) \sim z^{-1}$  and  $F_{ss}(z) \sim z^{-1}$ . Two simple contour integrals can be performed to verify that

$$\int_{-\infty}^{\infty} \rho_d(E) dE = 10 \quad (2.33)$$

and

$$\int_{-\infty}^{\infty} \rho_s(E) dE = 2. \quad (2.34)$$

A sum rule for  $\text{Im}\Sigma_d$  may also be easily derived. In this and other connections it is convenient to choose for the  $d$  resonance energies an energy origin such that

$$\epsilon_d^A = -\epsilon_d^B = \frac{1}{2}\Delta, \quad (2.35)$$

where

$$\Delta \equiv \epsilon_d^A - \epsilon_d^B. \quad (2.36)$$

From (2.20) and the asymptotic behavior of  $F_{dd}(z)$ , it can be seen that  $[\Sigma_d(z) - \bar{\epsilon}_d] \rightarrow xy\Delta^2 z^{-1}$ , as  $z \rightarrow \infty$ . Because  $\Sigma_d(z)$  is analytic in each half-plane, it follows that

$$\pi^{-1} \int_{-\infty}^{\infty} \text{Im}\Sigma_d(E + i0) dE = -xy\Delta^2. \quad (2.37)$$

From (2.31) it is seen that the quantity

$$\Sigma_s(z) \equiv \bar{\gamma}^2 (z - \Sigma_d)^{-1} \quad (2.38)$$

plays the role of the  $s$ -electron self-energy. The imaginary part of  $\Sigma_s$  may be associated with an inverse relaxation time of  $s$  electrons. This will be nonvanishing only at those energies for which  $\text{Im}\Sigma_d$  is nonzero. The  $s$  electrons are thus scattered as a consequence of the random positions of the  $d$  levels.

A decomposition of the average density of  $d$  states into  $A$  and  $B$  component densities<sup>1,2</sup> is also useful. From Eq. (2.19) it follows that

$$\rho_d(E, \Sigma_d) = x\rho_d^A(E, \Sigma_d) + y\rho_d^B(E, \Sigma_d), \quad (2.39)$$

where

$$10^{-1} \rho_d^{A,B}(E, \Sigma_d) = -\pi^{-1} \text{Im} \langle n_d = 0 | \langle (E^+ - H^{A,B})^{-1} \rangle | n_d = 0 \rangle, \quad (2.40)$$

and  $H^{A,B}$  is the Hamiltonian corresponding to a given alloy configuration with atoms of type  $A$  or type  $B$ , respectively, located at site  $n=0$ . Thus Eq. (2.40) may be written

$$\begin{aligned} 10^{-1} \rho_d^{A,B}(E, \Sigma_d) \\ = -\pi^{-1} \text{Im} \{ F_{dd} [1 - (\epsilon_d^{A,B} - \Sigma_d) F_{dd}]^{-1} \}_{z=E+i0} \end{aligned} \quad (2.41)$$

in an analogous fashion to Eq. (4.15) of Ref. 1.

This decomposition will be particularly useful in understanding the dilute-alloy limit.

Although, in general, Eq. (2.20) cannot be solved in closed form, several limiting cases may be easily investigated. These are (i) the dilute-alloy limit ( $x \approx 0$  or  $x \approx 1$ ); (ii) the atomic limit,  $\bar{\gamma} = 0$ ; (iii) the split- $d$ -band limit  $|w_s \Delta| \gg \bar{\gamma}^2$ .

#### B. Dilute-Alloy Limit

In the dilute alloy  $A_x B_{1-x}$  ( $x \approx 0$ ), it is useful to examine the average component densities  $\rho^A(E)$  and  $\rho^B(E)$ . From Eq. (2.41) it follows that

$$\rho_d^B(E, \Sigma_d) \approx \rho_d^B(E, \epsilon_d^B) \quad (2.42)$$

and

$$10^{-1}\rho_d^A(E, \Sigma_d) \cong -\pi^{-1} \text{Im}\{F_{dd}(E^+, \epsilon_d^B)/[1 - \Delta F_{dd}(E^+, \epsilon_d^B)]\}, \quad (2.43)$$

where the argument  $\epsilon_d^B$  is now given explicitly to show that  $F_{dd}$  and  $\rho_d$  are the pure host quantities. The average density of states  $\rho_d^A(E)$  may be written, using (2.43) and (2.24),

$$10^{-1}\rho_d^A(E) = -\pi^{-1} \text{Im}\left(\frac{1 + \bar{\gamma}^2(E - \epsilon_d^B)^{-1} F_{0s}[\epsilon_d^B - \bar{\gamma}^2(E - \epsilon_d^B)^{-1}]}{E - \epsilon_d^A - \Delta \bar{\gamma}^2(E - \epsilon_d^B)^{-1} F_{0s}[\epsilon_d^B - \bar{\gamma}^2(E - \epsilon_d^B)^{-1}]}\right). \quad (2.44)$$

For  $E$  near  $\epsilon_d^A$ , Eq. (2.44) becomes

$$10^{-1}\rho_d^A(E) = \frac{\bar{\gamma}^2 \rho_{0s}[E - \bar{\gamma}^2(E - \epsilon_d^B)^{-1}]}{\{E - \epsilon_d^A - \bar{\gamma}^2 \text{Re}F_{0s}[E - \bar{\gamma}^2/(E - \epsilon_d^B)]\}^2 + \{\pi \bar{\gamma}^2 \rho_{0s}[E - \bar{\gamma}^2/(E - \epsilon_d^B)]\}}. \quad (2.45)$$

If  $\rho_{0s}[E - \bar{\gamma}^2(E - \epsilon_d^B)^{-1}]$  is slowly varying with  $E$  near  $\epsilon_d^A$ , Eq. (2.45) indicates that  $\rho_d^A(E)$  is Lorentzian near  $\epsilon_d^A$ . Equation (2.45) is similar to the result found for the  $d$ -electron density associated with an impurity site in the Anderson-model Hamiltonian in which Coulomb interactions are neglected.<sup>16</sup> The essential difference is that in the present case, the hybridized host  $s$  band  $F_{0s}[E - \bar{\gamma}^2(E - \epsilon_d^B)^{-1}]$  appears in (2.45) in place of  $F_{0s}(E)$ . This is to be expected since the Anderson model assumes that the host band is pure  $s$  in character, whereas in noble-metal alloys the host has  $d$  electrons as well, which hybridize with the host  $s$  band.

The resonant state density about  $\epsilon_d^A$  mentioned above should be contrasted with the zero in the host-component density  $\rho_d^B(E, \epsilon_d^B)$  at the atomic level  $\epsilon_d^B$ . This zero in the density arises because there are sufficiently many  $d$  levels at energy  $\epsilon_d^B$  to hybridize with the  $s$  band throughout the crystal. However, in the dilute case there are far too few  $d$  levels at  $\epsilon_d^A$  to give rise to a gap in the  $s$  band near  $\epsilon_d^A$ . In other words, instead of a "hybridization resonance" there is an "Anderson resonance" at the impurity  $d$  level.

#### C. Atomic Limit ( $\bar{\gamma} = 0$ )

In the absence of hybridization and for  $\Delta \neq 0$ , we obtain results corresponding to the atomic limit that were previously discussed in Ref. 1 [Eqs. (4.21) and (4.26)]. The CPA equation (2.21) for  $\Sigma_d$  can be solved in closed form:

$$\Sigma_d = \bar{\epsilon}_d + xy\Delta^2/(z + \bar{\epsilon}_d). \quad (2.46)$$

Using (2.24) we have

$$F_{dd}(z) = (z - \Sigma_d)^{-1} \quad (2.47)$$

$$= (z + \bar{\epsilon}_d)/(z^2 - \bar{\epsilon}_d^2 - xy\Delta^2). \quad (2.48)$$

$F_{dd}(E)$  has poles at the two energies  $E = \pm \frac{1}{2}\Delta$  which coincide with the atomic energy levels  $\epsilon_d^A$  and  $\epsilon_d^B$ . In addition, Eq. (2.46) indicates that  $\Sigma_d$  also has a pole which is located at  $-\bar{\epsilon}_d$ . The density of  $d$  states in the atomic limit thus consists of two  $\delta$  functions located at  $\epsilon_d^A$  and  $\epsilon_d^B$ . The imaginary part of  $\Sigma_d$  has its entire weight at  $-\bar{\epsilon}_d$ , where the  $d$

spectral density is zero. It may be seen to satisfy the sum rule, Eq. (2.37).

#### D. Split- $d$ -Band Limit

The conditions under which a split- $d$ -band limit may exist in the presence of hybridization will now be examined. The criterion introduced in Ref. 1 for this condition was that  $\Sigma_d$  have a pole in a region of zero spectral density. As will be seen, this must be generalized for the present model Hamiltonian (2.8). We begin by investigating the conditions under which  $\Sigma_d(z)$  assumes the form

$$\Sigma_d(z) = A(z - a)^{-1} \text{ for } z \approx a. \quad (2.49)$$

For  $z$  arbitrarily close to  $a$  [ $\Sigma_d(z)$  large], it follows from (2.24) that  $F_{dd}(z)$  may be written

$$\begin{aligned} F_{dd}(z) &\sim (z - \Sigma_d)^{-1} + \bar{\gamma}^2(z - \Sigma_d)^{-2} F_{0s}(a) \\ &\quad - \bar{\gamma}^4(z - \Sigma_d)^{-3} \frac{\partial F_{0s}(a)}{\partial a} + \dots \\ &\equiv \sum_{p=0}^{\infty} (z - \Sigma_d)^{-p-1} \mu_p. \end{aligned} \quad (2.50)$$

It can be verified that a self-consistent assumption for the parameters of interest here is

$$F_{0s}(a) = O(1/w_s). \quad (2.51)$$

Following the arguments of Ref. 1, it may be seen that the relevant expansion parameter in investigating the split-band limit is  $(\mu_2/\Delta^2)^{1/2} = O(\bar{\gamma}^2/w_s\Delta)$ . Neglecting terms of order  $(\bar{\gamma}^2/w_s\Delta)^2$ , it follows from (2.20) that for  $z \cong a$

$$\Sigma_d(z) \cong xy\Delta^2/[z + \bar{\epsilon}_d - \bar{\gamma}^2 F_{0s}(a)], \quad (2.52)$$

where

$$a \equiv -\bar{\epsilon}_d + \bar{\gamma}^2 F_{0s}(a). \quad (2.53)$$

Equation (2.51) may now be explicitly verified using dimensional arguments and Eqs. (2.25) and (2.53). The arguments used to obtain (2.52) are the same as those used to derive Eq. (4.37) of Ref. 1, which deals with the single-band case. It should be noted that  $|\bar{\gamma}^2/w_s\Delta|$  is an oversimplification of the appropriate expansion parameter which is, nevertheless, suitable for the present discussion.

If  $|\bar{\gamma}^2/w_s\Delta| \ll 1$ , then  $a$  is between the two atomic

$d$  levels  $\epsilon_d^A$  and  $\epsilon_d^B$ . If the two levels are both inside the  $s$  band [ $\text{Im}F_{0s}(a) \neq 0$ ], a resonance in  $\Sigma_d$  will exist. If one of the levels lies outside the  $s$  band and  $|\bar{\gamma}^2/w_s\Delta| \ll 1$ , a pole will always form for some concentration  $x$ . For noble-metal alloys whose resonant  $d$  levels always lie inside the unhybridized  $s$  band there will never be a pole in  $\Sigma_d$ , even for very large  $\Delta$ . Throughout this paper, attention will be focused on the latter case which is appropriate for the noble metals.

Equations (2.52) and (2.37) may be used to show that because Eq. (2.52) nearly exhausts the sum rule for  $z$  near  $-\bar{\epsilon}_d$  (and  $|\bar{\gamma}^2/w_s\Delta| \ll 1$ ), it describes  $\text{Im}\Sigma_d(z)$  for all  $z$ .  $\text{Re}\Sigma_d(z)$  may be obtained from the Kramers-Kronig relation

$$\Sigma_d(z) = \bar{\epsilon}_d + \pi^{-1} \int_{-\infty}^{\infty} dE (E - z)^{-1} \text{Im}\Sigma_d(E^+). \quad (2.54)$$

An approximate expression for the self-energy, valid for the entire range of  $z$  when  $|\bar{\gamma}^2/w_s\Delta| \ll 1$ , is therefore

$$\Sigma_d(z) \cong \bar{\epsilon}_d + xy\Delta^2/[z + \bar{\epsilon}_d - \bar{\gamma}^2 F_{0s}(a)]. \quad (2.55)$$

As in the atomic limit,  $\rho_d$  has two sharp peaks centered at the  $d$  resonance levels  $\epsilon_d^A$  and  $\epsilon_d^B$ , near which  $\text{Im}\Sigma_d$  is almost zero. Although the value of  $\bar{\gamma}^2/w_s\Delta$  for which the  $d$  bands "split" must be determined numerically, a split- $d$ -band limit may, in general, be defined to exist when the imaginary part of the self-energy is concentrated as a resonance in a region where the density of  $d$  states is nearly zero. Under these circumstances the two  $d$  levels are essentially independent of one another. In summary this split- $d$ -band limit differs from that discussed in Ref. 1 in two ways: (a) There is no zero in the density of states between  $\epsilon_d^A$  and  $\epsilon_d^B$  because of hybridization with the  $s$  electrons; (b) there is no pole in  $\text{Im}\Sigma_d$  at  $-\bar{\epsilon}_d$ , but instead a well-defined resonance.

### III. APPLICATION TO Au-Ag

This section is divided into three parts. Sec. IIIA contains a brief description of some relevant aspects of the electronic properties of the pure metals Au and Ag. Some recent band calculations<sup>3</sup> for both Au and Ag will be summarized and a brief description of a renormalized atom theory,<sup>8</sup> which may be used to construct crystal potentials, will be presented.

Section IIIB will outline some relevant physical ideas concerning Au-Ag alloys. In Sec. IIIC a model for these alloys based on Eq. (2.8), as well as the choice of alloy parameters, will be discussed.

#### A. Pure Metals Au and Ag

Because of the difficulty in performing relativistic band calculations, the band theory for Au and Ag is not completely adequate. However, some reasonably reliable results for the band structure

are available. Table I summarizes the results of quasirelativistic APW band calculations to be used here.<sup>3,20</sup> It is seen that the Fermi energy in Au is 2.58 eV higher than in Ag. The bottom of the  $s$  band in Ag ( $\Gamma_1^{Ag}$ ) falls about 1.3 eV below that of Au ( $\Gamma_1^{Au}$ ). The occupied portion of the  $s$  band in Au,  $E_F^{Au} - \Gamma_1^{Au}$ , is thus 1.2 eV larger than  $E_F^{Ag} - \Gamma_1^{Ag}$ . The  $d$  bandwidth [ $E(X_5) - E(X_3)$ ] in Au is 5.4 eV; in Ag it is 3.8 eV. These values for the widths agree quite well with recent photoemission data.<sup>21</sup> The states at the top of the  $d$  band, involved in the first optical-absorption edge, lie energetically close to  $L_{32}$ . This level lies 2.19 eV below  $E_F^{Au}$  in Au and 4.06 eV below  $E_F^{Ag}$  in Ag. These values should be compared with 2.5 and 3.9 eV found experimentally for the edge.

It has been pointed out<sup>8</sup> that the  $d$  resonance energy  $\epsilon_d$  appearing in the Heine-Hubbard theory may be calculated from a renormalized atom point of view. The renormalized atom description, from which  $l$ -dependent Hartree-Fock crystal potentials may be derived, involves cutting off the free-atom  $s$  and  $d$  wave functions at the Wigner-Seitz radius and renormalizing them to a Wigner-Seitz sphere. The charge density obtained in this way may then be used to compute the potential. For noble metals this renormalization increases the  $d$  charge inside the sphere by less than 5%. However, it increases the  $s$  charge by roughly a factor of 2 to 3 in Cu and Ag. The change in  $\epsilon_d$  resulting from renormalization of the  $s$  wave functions is as follows:

$$\begin{aligned} \Delta\epsilon_d^{s-d} = & e^2 \int \int d\vec{r} d\vec{r}' |\psi_s(r)|^2 |\phi_d(r')|^2 |\vec{r} - \vec{r}'|^{-1} \\ & - e^2 \int \int d\vec{r} d\vec{r}' |\phi_s(r)|^2 |\phi_d(r')|^2 |\vec{r} - \vec{r}'|^{-1} \\ & + \text{exchange terms}, \quad (3.1) \end{aligned}$$

where  $\psi_s(r)$  is the renormalized atom  $s$ -electron

TABLE I. Band parameters for Ag and Au (see Ref. 3). (Energies in Ry relative to atomic zero.)

Energy	Ag	Au
Muffin-tin energy	-0.752	-0.682
$E_F$	-0.19	0.00
$\Gamma_1$	-0.707	-0.613
$\Gamma_{25}'$	-0.636	-0.372
$\Gamma_{12}$	-0.554	-0.255
$X_{11}$	-0.767	-0.567
$X_3$	-0.754	-0.534
$X_2$	-0.491	-0.161
$X_5$	-0.473	-0.134
$X_4'$	-0.019	+0.108
$L_{11}$	-0.735	-0.534
$L_{31}$	-0.640	-0.381
$L_{32}$	-0.490	-0.161
$L_2'$	-0.197	-0.078
$L_{12}$	+0.142	+0.408
$K_4$	-0.537	-0.237

wave function and  $\phi_{s,d}(r)$  represents the atomic  $s$  or  $d$  wave functions. As a result of the increased  $s$  charge density,  $\epsilon_d$  is increased by about 0.29 Ry in Ag and 0.23 Ry in Au from the free-atom values.<sup>8</sup> In addition, the  $d$  electrons repel one another more effectively than in the free atoms, thus increasing  $\epsilon_d$  by another 0.2 Ry. The  $d$ -level positions for<sup>22</sup> Ag obtained in this way are in good agreement with those determined from a first-principles APW calculation, based on an  $l$ -dependent renormalized atom potential when the center of gravity of the  $d$  bands,  $\frac{3}{5}E(\Gamma_{25'}) + \frac{2}{5}E(\Gamma_{12})$ , is associated with the resonance energy  $\epsilon_d$ . From the band calculations summarized in Table I, it is seen that  $\frac{3}{5}E(\Gamma_{25'}) + \frac{2}{5}E(\Gamma_{12})$  is 1.42 eV above  $\Gamma_1^{\text{Ag}}$  in Ag and 3.94 eV above  $\Gamma_1^{\text{Au}}$  in Au.

### B. Au-Ag Alloy System

It has been suggested<sup>6</sup> that the Wigner-Seitz cells in Au-Ag alloys are not neutral. Some experimental evidence for this comes from isomer-shift data of dilute Au in Ag which indicates that the  $s$  charge density at the Au nucleus in the alloy is different from that in pure Au.<sup>7</sup> In addition, ordered states are observed in a similar noble-metal alloy system  $\text{Au}_x\text{Cu}_{1-x}$  for concentrations of  $x=0.25$  and 0.5. The binding energy of ordered states has been ascribed to a Madelung energy associated with charged atoms.<sup>23</sup>

From the  $d$ -band calculations summarized in Table I, it was seen that the Fermi energy of pure Au is higher than that of pure Ag. In the Thomas-Fermi model of the alloy a difference in the Fermi energies of the alloy constituents will give rise to a charge transfer. This can be seen for dilute Ag in Au as follows: In the Thomas-Fermi model it is assumed that Ag electrons in an Au host have initially a Fermi energy  $E_F$  equal to that in pure Ag. When the alloy reaches equilibrium  $E_F$  must be uniform throughout and equal to the host Fermi energy in the dilute alloy. Since  $E_F^{\text{Au}} > E_F^{\text{Ag}}$ , conduction electrons are transferred from the Au host to the Ag impurity atoms. A charge transfer from Au to Ag will clearly also occur for dilute Au in Ag by the same reasoning. By contrast, Mott<sup>6</sup> has presented arguments to show that in dilute Au-Ag alloys there must be a net transfer of charge in the opposite direction. Since no band calculations for Au and Ag were available at the time it was supposed that because Au has a larger ionization potential, it should present a more attractive potential than Ag for the conduction-band electrons. This view seems to have been held by other investigators<sup>7,9,10</sup>; in particular, in connection with the isomer-shift data already discussed in the Introduction.

In this light our results might properly be regarded as controversial. It will be demonstrated,

however, in Sec. IV that good qualitative agreement between a model calculation of the concentration dependence of the optical-absorption edge and the experimental data is obtained only if Au loses electrons to Ag. On the other hand, very poor agreement is obtained if the charge is transferred in the opposite direction, as has been commonly assumed.

### C. Model for $\text{Au}_x\text{Ag}_{1-x}$

In this section a physical picture of the Au-Ag alloy system is developed which is expected to display some of its salient qualitative features. Equation (2.8) is proposed as a model Hamiltonian for the alloy. The parameters appearing in Eq. (2.8) are determined using the band-structure calculations of Table I. The renormalized atom theory,<sup>8</sup> described in Sec. IIIA, is applied to obtain the concentration dependence of  $\epsilon_d^{\text{Ag}}(x)$  and  $\epsilon_d^{\text{Au}}(x)$  using the notion of  $s$  charge transfer introduced in Sec. II. (The following convention will be adopted for notational convenience: When the argument  $x$  is omitted from  $\epsilon_d$ , the quantity  $\epsilon_d$  is to be taken as characteristic of the pure system; if the argument is included, it is to be taken as characteristic of the alloy.)

The choice of parameters for the pure systems will now be summarized.

(i) The unhybridized  $s$ -band density of states is assumed to have the simple shape discussed in Ref. 1:

$$\rho_{0s}(E) = (2/\pi w_s^2) (w_s^2 - E^2)^{1/2} - w_s \leq E \leq w_s \quad (3.2)$$

for both Au and Ag. The half-bandwidth is  $w_s = 7$  eV. This value of  $w_s$  is chosen to yield agreement with specific-heat data (neglecting all but the electronic contributions) and to give values of  $E_F^{\text{Ag}} - \Gamma_1^{\text{Ag}}$  and  $E_F^{\text{Au}} - \Gamma_1^{\text{Au}}$ , in reasonable accord with band-structure calculations. This will be discussed in more detail in Sec. IVA. It may be seen from (3.2) that the unhybridized  $s$  band is flat and broad, and not unlike a free-electron band for energies  $E$  less than or equal to the Fermi energies appropriate to Au and Ag. The effective mass at  $E = -w$  is  $0.88m_0$ . This choice for  $\rho_{0s}$  was made in order to simplify the numerical work. Because of the behavior of  $F_{dd}(z, \epsilon_d)$  for  $z = \epsilon_d$  discussed in connection with Eq. (2.24), it is necessary to expand  $F_{dd}(\epsilon_d, \epsilon_d)$  in order to subtract two canceling poles arising from the two terms in that equation. The calculations are considerably facilitated if  $F_{dd}(z, \epsilon_d)$ , or equivalently  $\rho_{0s}(E)$ , can be written in closed form. Equation (3.2) represents a simplification of the  $s$  band which is not justified in performing a transport calculation. However, as will be seen in Sec. IV, the behavior of the optical edge which is of interest here is fairly insensitive to the shape of the  $s$  band, particularly above  $E_F$ .

(ii) The  $d$  resonance levels measured with respect to the appropriate  $\Gamma_1$ 's are assumed to be  $\epsilon_d^{A^g} = 2.7$  eV,  $\epsilon_d^{Au} = 4.0$  eV. These values may be compared with  $\epsilon_d^{A^g} = 1.42$  eV and  $\epsilon_d^{Au} = 3.94$  eV taken from the band calculations summarized in Table I. It is seen that the value assigned to  $\epsilon_d^{A^g}$  is somewhat larger than the band calculations suggest. However, as will be seen in Sec. IV this adjustment is necessary in order to fit the experimentally observed optical-absorption edge in pure Ag with the model calculation of the edge. The discrepancy between the absorption edge calculated in the model with  $\epsilon_d^{A^g} = 1.4$  eV and that found from the band calculations summarized in Table I may in part be due to the difference in the values of the  $d$  bandwidth resulting from these two approaches.<sup>24</sup> The Ag  $d$  band in the model is considerably narrower (by about a factor of 2) than band theory and experiment predict.

(iii) The bottom of the  $s$  bands  $\Gamma_1^{Au}$  and  $\Gamma_1^{A^g}$  are assumed to be 1.36 eV apart;  $\Gamma_1^{A^g}$  is below  $\Gamma_1^{Au}$ . This separation for the  $\Gamma_1$ 's is taken from the band calculations summarized in Table I.

(iv) The hybridization constant is taken to be  $\gamma = \gamma^{Cu}(\epsilon_d/\epsilon_d^{Cu}) = 0.31\epsilon_d$ , when the values for Cu are obtained from Ref. 12.<sup>25</sup> It should be noted that in the Heine-Hubbard theory<sup>13,14</sup> for the band structure of Cu, the  $\gamma$  is assumed to be small. Consequently, a scaling of  $\gamma$  based on the Cu value is questionable for systems with broad  $d$  bands such as Au. It does, however, lead to results consistent with the band-calculation predictions for the number of  $d$  electrons above  $E_F$  in both Au and Ag when  $w_s = 7$  eV. This point will be discussed in Sec. IV A.

The choice of parameters appearing in Eq. (2.8) for the alloy system  $Au_xAg_{1-x}$  may be summarized as follows:

(i) In analogy with Ref. 1, the unhybridized  $s$ -band density of states in Au-Ag is the same as in pure Au and Ag and thus assumed to be  $\rho_{0s}(E)$  defined in Eq. (3.2). (ii) The  $d$  resonance energies will be assumed to be  $x$  dependent. Their  $x$  dependence will be described below. (iii) The unhybridized  $s$  band is described in a virtual-crystal model. The bottom of the  $s$  band is thus

$$\bar{\Gamma}_1 = x\Gamma_1^{Au} + y\Gamma_1^{A^g}, \quad (3.3)$$

and (iv) the hybridization constant  $\gamma$  will be evaluated at  $\bar{\epsilon}_d = x\epsilon_d^{Au} + y\epsilon_d^{A^g}$ .

The remainder of this section will be devoted to determining the  $x$  dependence of  $\epsilon_d^{Au}(x)$  and  $\epsilon_d^{A^g}(x)$  as measured with respect to  $\Gamma_1^{Au}$  and  $\Gamma_1^{A^g}$ , respectively.

The notion of  $s$  charge transfer was motivated using a Thomas-Fermi picture for the dilute alloy. The same considerations are expected to apply in the nondilute case as well. It is clear that the average charge  $\Delta Q$  associated with an Au or an Ag atom is dependent on the concentration of each type

of atom in the alloy. The impurity atoms in the very dilute alloys ( $x \approx 0$ ,  $x \approx 1$ ) are expected to have a greater absolute value of charge per atom than the host atoms because the impurities are surrounded by more atoms of unlike character. To determine the  $x$  dependence of  $\Delta Q^{Au}$  and  $\Delta Q^{A^g}$  for nondilute alloys, it appears to be reasonable to interpolate linearly between the dilute-alloy limits. Some experimental evidence supporting this point of view will be mentioned subsequently. We shall thus assume that the  $s$  dependence of  $\Delta Q^{Au, A^g}$  is of the form

$$\Delta Q^{Au}(x) = y\Delta Q^{Au}(x \approx 0) \quad (3.4)$$

and

$$\Delta Q^{A^g}(x) = x\Delta Q^{A^g}(x \approx 1), \quad (3.5)$$

where the arguments ( $x \approx 0$ ) and ( $x \approx 1$ ) indicate the appropriate dilute alloys.

The  $x$  dependence of  $\epsilon_d^{Au}(x)$  and  $\epsilon_d^{A^g}(x)$  may now be understood. The renormalized atom picture described previously suggests that a change in  $s$  charge density on an Au or Ag atom will significantly affect the position of the  $d$  resonance levels.<sup>8</sup> Consequently, if  $\Delta Q^{Au}(x)$  and  $\Delta Q^{A^g}(x)$  depend on  $x$ , then  $\epsilon_d^{Au}(x)$  and  $\epsilon_d^{A^g}(x)$  will also. Since the direct part of the  $s$ - $d$  Coulomb interaction dominates the exchange term,<sup>8</sup> the change in  $\epsilon_d^{A^g}$  resulting from a change in  $s$  charge density per atom  $\Delta Q^{A^g}$  is approximately

$$\begin{aligned} (\Delta\epsilon_d^{s-d})_{\text{direct}} \\ = e^{-1}\Delta Q^{A^g} \left[ \int \int d\vec{r} d\vec{r}' |\psi_s^{A^g}(r)|^2 |\phi_d^{A^g}(r')|^2 |\vec{r} - \vec{r}'|^{-1} \right], \end{aligned} \quad (3.6)$$

where  $\phi_d^{A^g}(r)$  represents the  $d$  atomic wave function of Ag, and  $\psi_s^{A^g}(r)$  is the renormalized atom  $s$  wave function associated with Ag atoms before the charge is transferred. The factor  $e^{-1}\Delta Q^{A^g}$  accounts for the fact that in the alloy  $\psi_s^{A^g}(r)$  is no longer normalized to unity within the Wigner-Seitz cell. Since the integral in (3.6) is the same as in pure Ag, it follows from the discussion in Sec. IIIA that if an average  $s$  charge per atom of  $\Delta Q^{A^g}(x)$  is added to Ag atoms in  $Au_xAg_{1-x}$ , the  $d$  level increases by

$$\Delta\epsilon_d^{A^g}(x) = e^{-1}\Delta Q^{A^g}(x) (0.29) \text{ Ry}. \quad (3.7)$$

Similarly, if an average  $s$  charge per atom of  $|\Delta Q^{Au}(x)|$  is subtracted from Au atoms in  $Au_xAg_{1-x}$ , the  $d$  level decreases by

$$\Delta\epsilon_d^{Au}(x) = -|e^{-1}\Delta Q^{Au}(x)| (0.23) \text{ Ry}. \quad (3.8)$$

Using Eqs. (3.4) and (3.5) and the neutrality condition

$$x\Delta Q^{Au}(x) + y\Delta Q^{A^g}(x) = 0, \quad (3.9)$$

it follows that

$$\Delta Q^{A^g}(x \approx 1) = -\Delta Q^{Au}(x \approx 0). \quad (3.10)$$

Thus (3.7) and (3.8) may be written in terms of one parameter,  $\Delta Q^{Ag}(x \approx 1)$ , to be called the charge-transfer parameter

$$\Delta \epsilon_d^{Au}(x) = -ye^{-1} \Delta Q^{Ag}(x \approx 1) \quad (0.23) \text{ Ry} \quad (3.11)$$

and

$$\Delta \epsilon_d^{Ag}(x) = xe^{-1} \Delta Q^{Ag}(x \approx 1) \quad (0.29) \text{ Ry} . \quad (3.12)$$

There is some experimental evidence to justify Eqs. (3.4), (3.5), and (3.10). The resistivities of  $\text{Au}_x\text{Ag}_{1-x}$  for the two dilute alloys ( $x \approx 1$ ,  $x \approx 0$ ) are equal,<sup>26</sup> as is consistent with (3.10).<sup>27</sup> In addition, Mössbauer experiments show a nearly linear dependence of the isomer shift of Au in Ag on concentration  $x$ .<sup>7</sup>

A Thomas-Fermi model may be adopted to give a rough estimate of the charge transfer to be expected in the two dilute cases ( $x \approx 0$ ,  $x \approx 1$ ). The charge transfer is computed from the following equations:

$$\begin{aligned} \Delta Q^{Ag}(x \approx 1) &= e \int_{-\infty}^{E_f^{Au}} \rho_s[E, \epsilon_d^{Ag}(x \approx 1)] dE \\ &\quad - e \int_{-\infty}^{E_f^{Ag}} \rho_s(E, \epsilon_d^{Ag}) dE \end{aligned} \quad (3.13)$$

and

$$\begin{aligned} \Delta Q^{Au}(x \approx 0) &= e \int_{-\infty}^{E_f^{Ag}} \rho_s[E, \epsilon_d^{Au}(x \approx 0)] dE \\ &\quad - e \int_{-\infty}^{E_f^{Au}} \rho_s(E, \epsilon_d^{Au}) dE . \end{aligned} \quad (3.14)$$

Using Eqs. (3.7) and (3.8) for  $x \approx 1$ , it is seen that the right-hand side of Eqs. (3.13) and (3.14) are implicit functions of  $\Delta Q^{Ag}(x \approx 1)$  and  $\Delta Q^{Au}(x \approx 0)$ , respectively. Using Eqs. (2.29), (2.31), and the pure-metal parameters discussed earlier, Eqs. (3.13) and (3.14) may be solved numerically to give

$$-\Delta Q^{Au}(x \approx 0) \approx \Delta Q^{Ag}(x \approx 1) = 0.3e . \quad (3.15)$$

This value is in unexpectedly good agreement with the results to be presented in Sec. IV B. In the applications considered here,  $\Delta Q^{Ag}(x \approx 1)$  will be assumed to be adjustable. The estimate of the charge-transfer parameter given in Eq. (3.15) will be used only as a guideline.

In addition to the assumptions stated in the text, there are two further effects not considered in the above estimate of the charge-transfer parameter which a more exact theory should contain. These are (a) the possibility of  $d$ -electron transfer and (b) the effect of  $s$ -electron transfer on  $\Gamma_1$ . The inclusion of either or both of these in the Fermi-Thomas calculations would tend to lower the value (0.3e) found for  $\Delta Q^{Ag}(x \approx 1)$ .

#### IV. NUMERICAL EXAMPLES FOR MODEL ALLOYS AND Au-Ag

This section is divided into two parts. In the first part some of the general results pertaining to the model Hamiltonians [Eqs. (2.1) and (2.8)] discussed in Sec. II A will be illustrated. The choice of pa-

rameters will generally be characteristic of Au-Ag alloys. Illustrations of the split- $d$ -band limit, however, will be concerned with alloy parameters different from those in Au-Ag. In Sec. IV B, the model-alloy Hamiltonian Eq. (2.8) and the CPA will be used to estimate the behavior of the optical-absorption edge for the first interband transition. The concentration dependence of the edge for several choices (both positive and negative) of the charge-transfer parameter  $\Delta Q^{Ag}(x \approx 1)$  will be investigated. The results obtained here for the behavior of the absorption edge are not expected to be qualitatively sensitive to the shape of the  $s$  and  $d$  bands (as contrasted to their relative positions and the  $d$  bandwidth), since interest is focused on the positions of the tops of the  $d$  bands relative to the Fermi energy. They are, however, very sensitive to the sign of the charge-transfer parameter, as will be demonstrated.

##### A. Numerical Examples

Figures 2(a) and 2(b) show the  $d$  and  $s$  densities of states for pure Ag and Au, respectively. The calculations were performed using the model Hamiltonian [Eq. (2.1)] and the parameters for pure Au and Ag discussed in Sec. III C. The quantities  $\rho_s$  and  $\rho_d$  were evaluated numerically using Eqs. (2.24), (2.27), (2.29), and (2.31) with  $\Sigma_d = \epsilon_d^{Ag, Au}$ .

As discussed in Sec. II A, an unphysical feature of the model Hamiltonian is the gap appearing in the density of states which contains the  $d$  resonance energy  $\epsilon_d$ . For the purposes of applying the model to compute the absorption edge as a function of  $x$ , the structure of the  $d$  band below its upper edge is expected to be unimportant. Such structural features as the gap in the  $d$  and  $s$  bands will be discussed in this section because they give insight into some of the important changes which occur in the densities of states with alloying.

Comparing Figs. 2(a) and 2(b), it is seen that there are several important differences in  $\rho_d$  for pure Ag and Au. These all derive from the change in  $\gamma$  with the position of the  $d$  resonance levels (measured with respect to the bottom of the  $s$  band) in these two systems. The  $d$  band in Au shown in Fig. 2(b) is  $\sim 2$  eV broader than that of pure Ag [Fig. 2(a)]. The gap in Au is several tenths of an eV wider than that in Ag. Both gaps, however, may be seen to contain the appropriate resonance level,  $\epsilon_d^{Au}$  or  $\epsilon_d^{Ag}$ .

Two characteristic features of  $\rho_d$ , present in both Figs. 2(a) and 2(b), are the large peaks in  $\rho_d$  on either side of the gap in the vicinity of the  $d$  resonance level and large "tails" in the  $d$ -band density of states. The latter are in sharp contrast to the nearly flat upper edges of the  $d$  bands actually found in noble metals.

The tails in  $\rho_d$  found from the model Hamiltonian

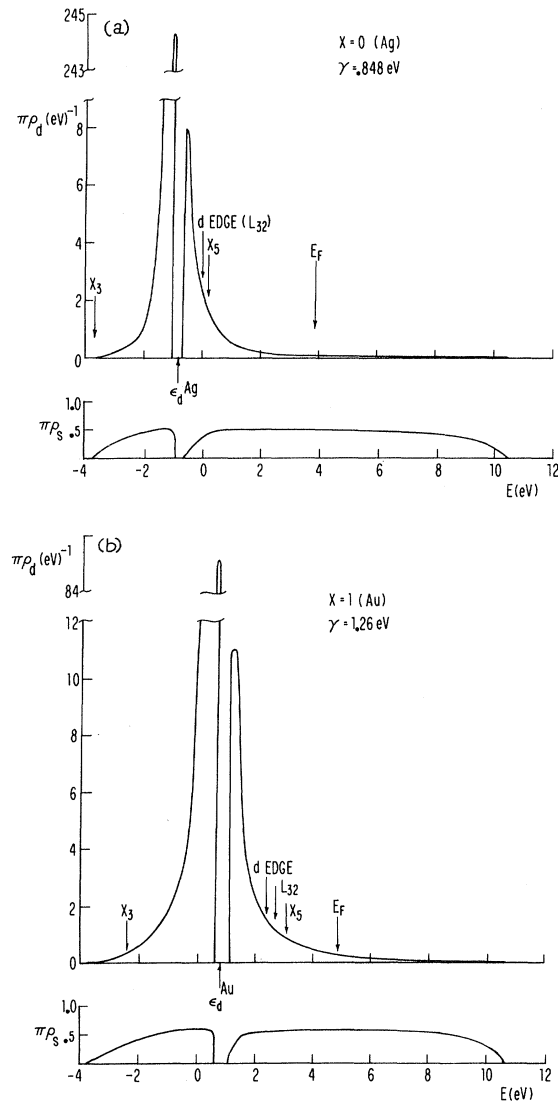


FIG. 2. Density of states for  $s$  and  $d$  bands for (a) Ag and (b) Au, calculated from Eq. (2.1). Hybridization constants  $\gamma$ ,  $d$  levels  $\epsilon_d$ , upper  $d$ -band edge, Fermi energy  $E_F$ , and energy positions of  $X_3$ ,  $X_5$ , and  $L_{32}$  obtained from band calculations (see Table I) are indicated. Here as in all figures, the energy origin is chosen so that  $\epsilon_d^{Au} = -\epsilon_d^{Ag}$ .

[Eq. (2.1)] result in a finite but small number of  $d$  electrons (0.07 in Ag and 0.18 in Au) above the Fermi energy  $E_F$ , and a finite density of  $d$  electrons at  $E_F$ . For the band calculations summarized in Table I, it was found that as a consequence of  $s$ - $d$  hybridization there are about 0.05  $d$  electrons in Ag and 0.14  $d$  electrons in Au above  $E_F$ .<sup>3</sup>

The absence of a flat  $d$  edge complicates an estimate of the optical-absorption edge for the first interband transition. Consequently, a cutoff for the  $d$  band must be determined somewhat arbitrarily.

The qualitative nature of the results is not, however, sensitively dependent on the cutoff criteria, provided the same criterion is used for all alloy concentrations. Two criteria, both chosen to fit the *pure-metal* absorption edges at 3.9 and 2.5 eV in Ag and Au, respectively, using the parameters of Sec. IIIC were found to give essentially the same results for the  $x$  dependence of the edge in the alloy. These were a cutoff of the  $d$  band at 93% of the total area and a cutoff of the band when the  $d$  density of states has fallen to 2% of its maximum value. In the remaining figures, discussed in the section, the cutoff is determined using the first of these. The  $d$ -band edges indicated in Fig. 2 nearly coincide with the positions of  $L_{32}$  obtained from band calculations for both Au and Ag when the Fermi energies in Figs. 2(a) and 2(b) are made to coincide with the Fermi energies in Table I.

Using the same criteria to assign a bottom edge to the  $d$  bands, it is found that the  $d$  widths for Ag and Au are, respectively, 1.8 and 3.1 eV, as contrasted to the values 3.8 and 5.4 eV associated with  $E(X_5) - E(X_3)$  in Table I. The separation of the Fermi energies and the bottom of the  $s$  bands in Fig. 2 are 7.65 and 8.55 eV for Ag and Au, respectively. These values are in reasonable agreement with the corresponding results 8.3 and 7.1 eV, given in Table I.

Focusing attention on the  $s$  bands in Fig. 2, it may be seen that their shapes are distorted in two important ways by hybridization effects. First, there are gaps in the density of  $s$  states about the  $d$  resonance levels  $\epsilon_d^{Au, Ag}$ , and second, the bottom of the  $s$  bands for Au and Ag are several tenths of an eV lower than in the absence of hybridization. The latter effect, which can be verified theoretically using Eqs. (2.29) and (2.31), is small compared to the total  $s$  bandwidth (14 eV) and will be neglected.

The total density of states at the Fermi energy, including the small  $d$  contribution, is  $0.211$  (eV<sup>-1</sup>) in Ag and  $0.268$  (eV<sup>-1</sup>) in Au. Specific-heat data suggest densities of  $0.26$  (eV<sup>-1</sup>) in Ag and  $0.303$  (eV<sup>-1</sup>) in Au.<sup>28</sup> Despite the neglect of dressing effects, the agreement is seen to be fairly good. This fact supports the choice of value of 14 eV chosen here for the total  $s$  bandwidth.

In the remainder of Sec. IVA, the results of the CPA applied to the *alloy* Hamiltonian Eq. (2.8) will be considered. The discussion will focus on the densities of states for several alloy concentrations and a charge-transfer parameter  $\Delta Q^{Ag}(x \approx 1) = 0.3e$ . The split- $d$ -band limit and the behavior of the imaginary part of  $\Sigma_d$  will also be illustrated.

Figure 3(a) shows the  $s$  and  $d$  densities for  $Au_{0.1}Ag_{0.9}$ . Although the impurity concentration  $x$  is not small, the results for the  $d$  density of states in the alloy can, nevertheless, be understood

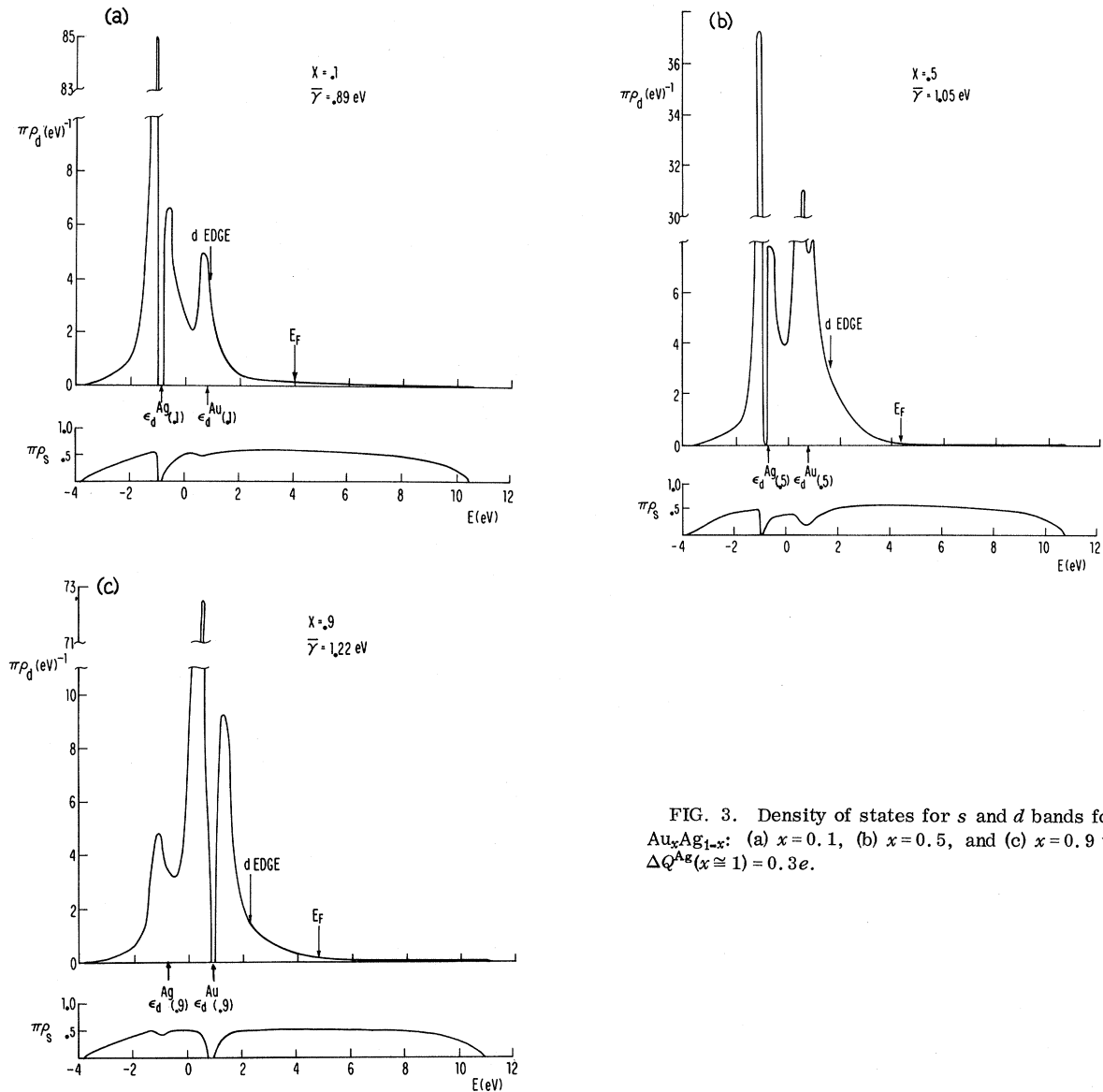


FIG. 3. Density of states for *s* and *d* bands for Au<sub>*x*</sub>Ag<sub>1-*x*</sub>: (a) *x*=0.1, (b) *x*=0.5, and (c) *x*=0.9 with  $\Delta Q^{Ag}(x \cong 1) = 0.3e$ .

by referring to the theoretical expressions for the dilute-alloy limit, Eqs. (2.42) and (2.45). The alloy *d* band is approximately a superposition of the pure Ag band and a broad *d* resonant state about the Au *d* level. The host *d* level has a gap associated with it, as in pure Ag; the impurity *d* level gives rise to a resonance, as in the Anderson-model Hamiltonian.<sup>16</sup>

The *s* band in the alloy differs from that in pure Ag, primarily for energies in the vicinity of  $\epsilon_d^{Au}(0.1)$ . It is seen that there is a small minimum in  $\rho_s$  near the impurity *d* level which may be associated with an increased *s-d* "interaction" analogous to hybridization effects which give rise to a gap in  $\rho_s$  near the host *d* level.

In Fig. 3(b), the *s* and *d* densities are exhibited

for the 50-50 alloy. It may be seen by comparing Figs. 3(a) and 3(b) that the density of *d* states near  $\epsilon_d^{Au}$  and  $\epsilon_d^{Ag}$  has now taken on features of both hybridization and Anderson-type resonances. The gap near  $\epsilon_d^{Ag}$  is narrower than in the previous figure, suggesting a trend toward a pure Anderson resonance at  $\epsilon_d^{Ag}$  as *x* increases. Near  $\epsilon_d^{Au}$ , a minimum in both  $\rho_s$  and  $\rho_d$  has appeared, characteristic of an incipient hybridization resonance. The *s* and *d* densities for *x*=0.9 are shown in Fig. 3(c). This figure is similar to Fig. 3(a), with the position of the Anderson and hybridization resonance levels interchanged.

The imaginary part of the self-energy  $\text{Im}\Sigma_d$  of Au<sub>*x*</sub>Ag<sub>1-*x*</sub> at two impurity concentrations, *x*=0.1 and 0.5 for a charge transfer [ $\Delta Q^{Ag}(x \cong 1)$ ] of 0.3e,

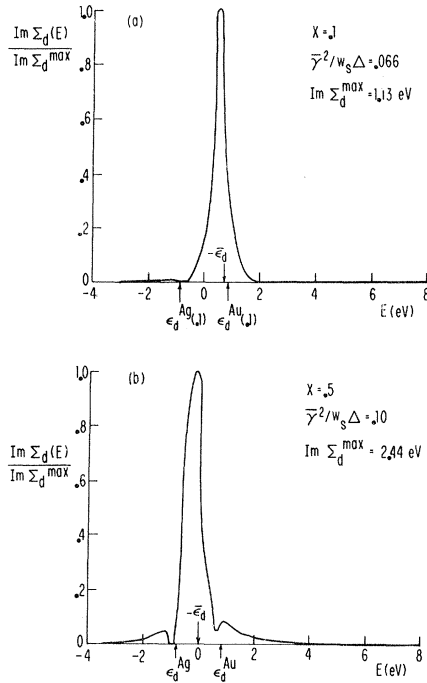


FIG. 4. Imaginary part of  $d$ -electron self-energy vs  $E$  for  $Au_xAg_{1-x}$ : (a)  $x=0.1$ , (b)  $x=0.5$  in units of its maximum amplitude.

is plotted in Fig. 4. These parameters correspond to those of the densities of states shown in Figs. 3(a) and 3(b). Comparing Fig. 4 with Figs. 3(a) and 3(b), it may be seen for both alloys that the damping is appreciable in an energy region where  $\rho_d$  is nonzero. It follows, then, that the two  $d$  levels are not independent of one another. For the parameters characteristic of Au-Ag ( $\bar{\gamma}^2/w_s\Delta \approx 0.1$ ), the  $d$  bands are clearly not "split" in the sense defined in Sec. IID. It is seen in Fig. 4(a) that for  $x=0.1$ , the weight of  $\text{Im}\Sigma_d$  is concentrated near the impurity atomic level  $\epsilon_d^{\text{Au}}$  (0.1); for  $x=0.5$  [Fig. 4(b)], the damping is roughly equally distributed about the two  $d$  levels, as expected. In both figures the maximum in  $\text{Im}\Sigma_d$  appears near the energy  $-\bar{\epsilon}_d$ . The shape of  $\text{Im}\Sigma_d$  is clearly not Lorentzian, as it would be if Eq. (2.52) were valid.

The remaining two examples in this section will be concerned with an artificial alloy  $A_xB_{1-x}$  in which the two  $d$  levels are at 2.94 and 9.24 eV above  $\Gamma_1$ . The concentration of the alloy is fixed at  $x=0.2$ . The alloy will be used to illustrate the split- $d$ -band limit (Sec. IID) which is attained when  $\bar{\gamma}$  is made sufficiently small.

Figure 5 shows the density of states for the  $d$  band in the model alloy for  $\bar{\gamma}=1.3$  eV. It is seen in Fig. 5(a) that, although the two  $d$  levels are

6.3 eV apart,  $\rho_d$  has the same structure as in Fig. 3. There is a gap in  $\rho_d$  at the host  $d$  level  $\epsilon_d^B$  and a resonance in  $\rho_d$  near the impurity level  $\epsilon_d^A$ . The density of states is small but finite in the energy region between the two atomic levels.

The results shown in Fig. 5(b) correspond to the same parameters, except that  $\bar{\gamma}$  (= 0.435 eV) is  $\frac{1}{3}$  smaller than in Fig. 5(a). The density of states in the alloy now assumes an "atomiclike" character, as expected from the discussion in Sec. IID. Although there is no gap at  $\epsilon_d^B$ , the effects of hybridization are non-negligible. The  $d$  levels at  $\epsilon_d^A$  and  $\epsilon_d^B$  are broadened relative to the atomic limit ( $\bar{\gamma}=0$ ) due to  $s$ -electron hybridization. In addition, there is a finite  $d$  density of states between the two  $d$  levels as a result of hybridization.

Although the shape of  $\rho_d$  is different in both parts of Fig. 5, it will be seen by referring to the corresponding  $\text{Im}\Sigma_d$  plotted in Fig. 6 that both alloys may be said to be to a greater or lesser extent in a split- $d$ -band limit. In Fig. 6(a) the parameter  $\bar{\gamma}^2/w_s\Delta$  is 0.0375, or typically one-half as large as in Au-Ag alloys. The damping is nearly Lorentzian about  $-\bar{\epsilon}_d$ , as expected from the discussion in Sec. IID. Most of the weight of  $\text{Im}\Sigma_d$  is in a region of nearly zero spectral density. Thus the two  $d$  levels are almost, although not completely,

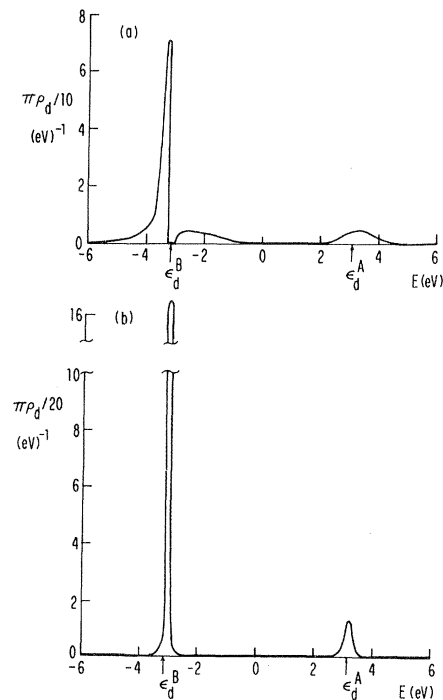


FIG. 5. Density of  $d$  states for artificial split- $d$ -band alloys  $A_{0.2}B_{0.8}$  having  $\epsilon_d^A=9.24$  eV and  $\epsilon_d^B=2.94$  eV. The hybridization constants are (a) 1.3 eV and (b) 0.435 eV.

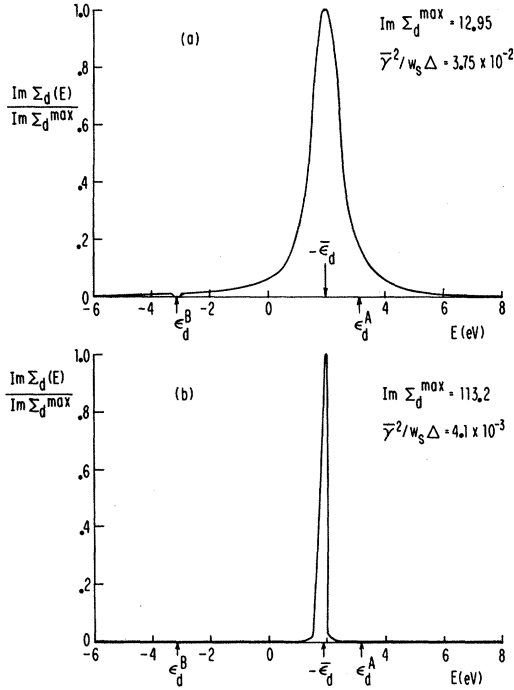


FIG. 6.  $\text{Im}\Sigma_d$  vs  $E$  in units of its maximum amplitude for the two alloys of Fig. 5.

independent of one another. This alloy, therefore, may be viewed as being on the edge of the split- $d$ -band limit. In Fig. 6(b), by contrast,  $\bar{\gamma}^2/w_s\Delta$  is about  $\frac{1}{10}$  as large as in Fig. 6(a). Here  $\text{Im}\Sigma_d$  is strongly peaked at  $-\bar{\epsilon}_d$ , the Lorentzian character being very marked. It is approximately zero at both atomic  $d$  levels  $\epsilon_d^A$  and  $\epsilon_d^B$ . Accordingly, this alloy is clearly in a split- $d$ -band limit. This type of split-band behavior was discussed in Ref. 1 for a single-band alloy. In the latter case the bands were split and a pole appeared in  $\text{Im}\Sigma$  when  $|\epsilon^A - \epsilon^B|$  was about equal to the half-bandwidth. By contrast, in the two-band model the analogous split-band limit is considerably more restrictive and does not occur until  $|w_s\Delta/\bar{\gamma}^2|$  is about  $10^2$ . This can be seen physically as arising from the fact that the  $d$  bands effectively "interact" with one another, even though they may be situated quite far apart, as a result of hybridization with the  $s$  electrons.

Consequently, it is not correct, in view of the results of the model calculation, to assign split- $d$ -band behavior to noble-metal alloys on the basis of whether the  $d$  bands before alloying do or do not overlap with one another.<sup>14</sup> Furthermore, as will be seen in Sec. IVB, there is evidence that the positions of the  $d$  levels associated with Au and Ag in Au-Ag alloys may be quite different from those found in the pure metals Au and Ag.

#### B. Absorption Edge in $\text{Au}_x\text{Ag}_{1-x}$

In this section the concentration dependence of the position of the absorption edge for Au-Ag is discussed on the basis of the model Hamiltonian [Eq. (2.8)] using the alloy parameters given in Sec. III C. Four different values of the charge-transfer parameter will be considered:  $\Delta Q^{Ag}(x \approx 1) = 0, 0.3e, -0.2e,$  and  $0.5e$ .

The dashed line in Fig. 7(a) shows the experimentally observed optical-absorption edge for the first interband transition in Au-Ag alloys as a function of impurity concentration  $x$ . The data were taken from the position of the knee in reflectivity measurements.<sup>4</sup> The endpoints were fitted to the values of 2.5 eV for pure Au and 3.9 for pure Ag. The curve thus obtained is in reasonable agreement with the experimental results of Ref. 5.

Two important aspects of the behavior of the experimentally determined edge as a function of  $x$  should be noted here. First, the rate of change of the edge for dilute Au in Ag is many times larger than for dilute Ag in Au. Second, as Au is added to Ag, the edge shifts monotonically to lower energies. The former of these two qualitative effects was again verified recently.<sup>15,29</sup>

The first effect can be explained by the model calculation without reference to the concept of charge transfer. The second effect is explainable within the model only if  $s$  charge is transferred from Au to Ag atoms in Au-Ag alloys.

We now proceed to explain the first of these two qualitative observations. It may be seen from Fig. 3 that for all three concentrations considered, the upper-half of the  $d$  band, in particular the band edge, is determined primarily by the Au atoms, whose  $d$  level lies above that of Ag. These results are independent of the choice of  $\Delta Q^{Ag}(x \approx 1)$  as long as for all  $x$ ,  $E_F - \epsilon_d^{Ag} > E_F - \epsilon_d^{Au}$ . It is thus expected that for Ag-rich alloys ( $x \approx 0$ ) the position of the absorption edge as a function of  $x$  will rapidly decrease from its value in pure Ag as the Au  $d$  states begin to appear. By contrast, for Au-rich alloys the position of the top of the  $d$  band is determined by Au atoms for all  $x$  near 1. Consequently, for these alloys the position of the absorption edge is expected to be relatively constant with  $x$ .

The fact that it is not possible to explain the observed monotonic decrease of the edge position with increasing  $x$  without invoking the idea of transfer of  $s$  charge may be seen from Fig. 7(b) which shows the absorption edge as a function of  $x$  (solid line) when charge-transfer effects are neglected. This curve is clearly not monotonically decreasing with  $x$  as is the experimental one (dashed curve). According to the discussion of Sec. III C, the  $d$  levels  $\epsilon_d^{Au, Ag}$  in the alloy are the same as in the pure-metal systems in this case. Because the Au  $d$  level remains fixed at the energy  $\epsilon_d^{Au}$ , the only

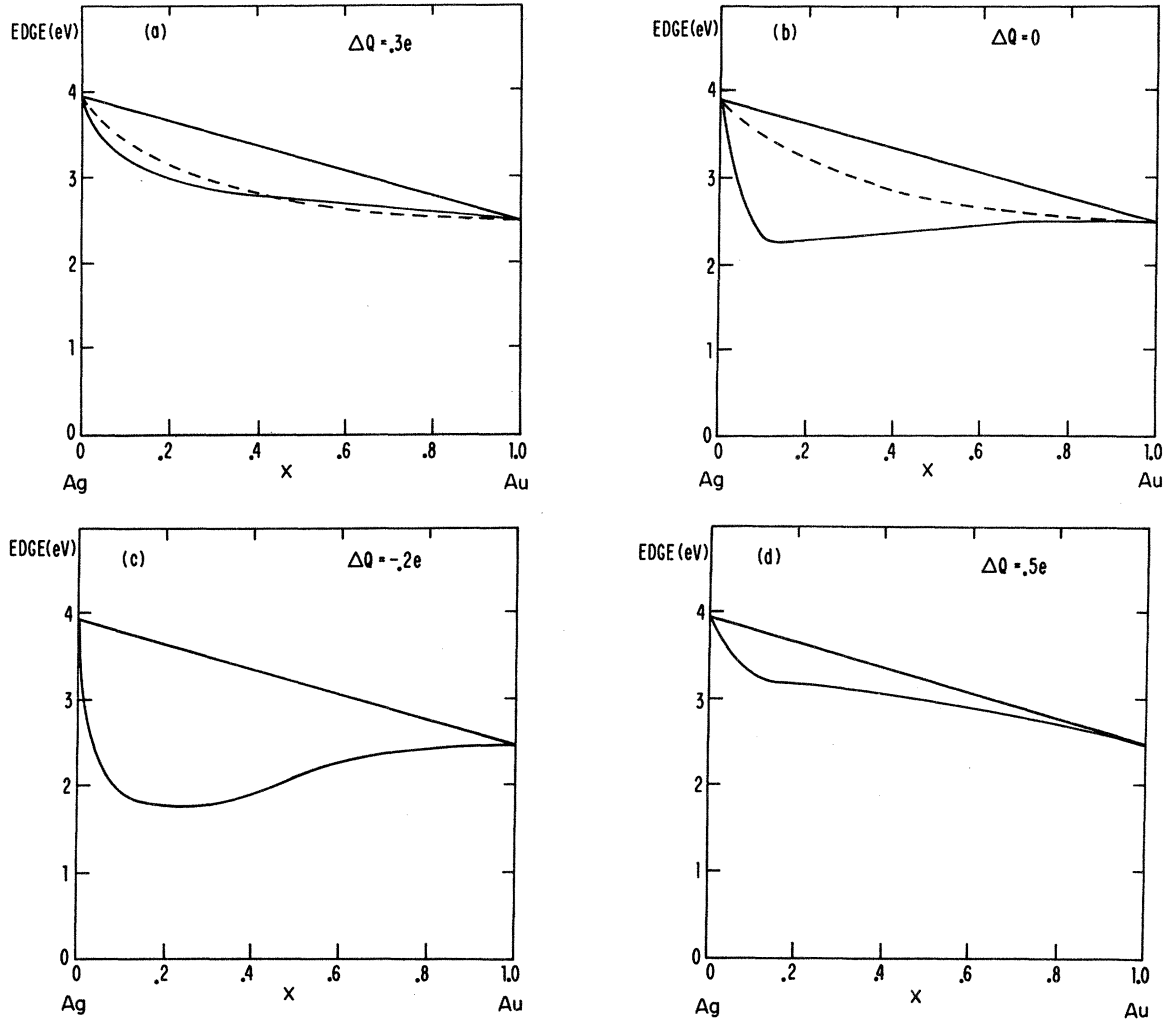


FIG. 7. Optical-absorption edge vs  $x$  for four values of  $\Delta Q^{Ag}(x \cong 1)$ : (a)  $0.3e$ ; (b)  $0$ ; (c)  $-0.2e$ ; and (d)  $0.5e$ . Dotted lines in the figures are the experimental curve.

changes in the position of the edge with alloying, for  $x$  away from zero and increasing, result from a broadening of  $\rho_d$  near  $\epsilon_d^{Au}$  and a concomitant increase in  $E_F$  which is associated with the fact that  $\rho_{0s}$  is reduced in the region where  $\rho_d$  is large. As is seen, these two effects nearly compensate for one another and give rise to an absorption edge which, except at very small  $x$ , is nearly constant with  $x$ .

It is therefore clear that the position of the Au  $d$  level  $\epsilon_d^{Au}$  must be concentration dependent. To ensure that the absorption-edge position decreases monotonically as Au is added to Ag, the parameter  $e^{-1}\Delta Q^{Ag}(x \cong 1)$  must in fact be *positive*.

The sketches in Fig. 8 serve to clarify this point. The position of the  $d$  levels  $\epsilon_d^{Au}$  and  $\epsilon_d^{Ag}$ , the Fermi energy, and the  $d$ -band edges for three different charge-transfer parameters  $-0.2e$ ,  $0$ ,

and  $0.3e$  for dilute Au in Ag ( $x = 0.1$ ) and for dilute Ag in Au ( $x = 0.9$ ) are illustrated in Figs. 8(a) and 8(b), respectively. For  $\Delta Q^{Ag}(x \cong 1) = -0.2e$  the Au  $d$  level is above pure Au for both concentrations. As seen in Figs. 8(a) and 8(b), for  $\Delta Q^{Ag}(x \cong 1) = 0.3e$ , the Au  $d$  level position is *below* that of pure Au for all concentrations. In this latter case, as  $x$  increases,  $\epsilon_d^{Au}(x)$  moves *up* toward the value  $\epsilon_d^{Au}$ , characteristic of the pure system [Figs. 8(b) and 8(c)]. The absorption edge thus monotonically *decreases* with  $x$ , as found experimentally. This behavior is expected for all  $e^{-1}\Delta Q^{Ag}(x \cong 1) < 0$ .

On the other hand, for  $\Delta Q^{Ag}(x \cong 1) = -0.2e$ , where the Au  $d$ -level position is *above* that of pure Au for all concentrations,  $\epsilon_d^{Au}(x)$  moves *down* toward the value  $\epsilon_d^{Au}$  with increasing  $x$ . Except at small  $x$ , the absorption edge increases monotonically, contrary to experiment. This behavior is expected

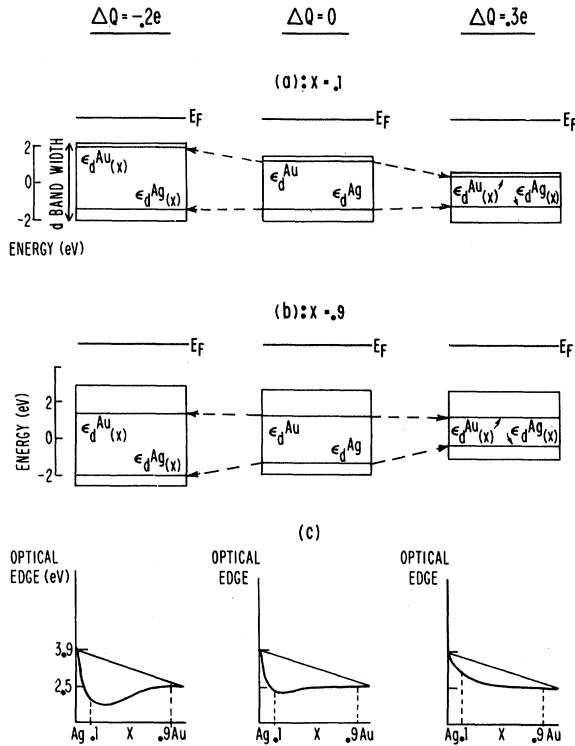


FIG. 8. Schematic representation of  $d$ -band positions for three values of  $\Delta Q^{Ag}(x \cong 1)$  and two alloy concentrations: (a)  $x=0.1$  and (b)  $x=0.9$ . (c) Qualitative  $x$  dependence of the optical-absorption edge for the three  $\Delta Q^{Ag}(x \cong 1)$ .

for all  $e^{-1}\Delta Q^{Ag}(x \cong 1) > 0$ . For  $e^{-1}\Delta Q^{Ag}(x \cong 1) = 0$ , the behavior is seen to be intermediate between that found for the two choices of charge-transfer parameter just discussed.

The validity of these remarks will now be substantiated by examining in more detail the  $x$  dependence of the edge calculated on the basis of the present model for three nonzero values of  $\Delta Q^{Ag}(x \cong 1) = 0.3e$ ,  $-0.2e$ , and  $0.5e$ . The best value for the charge-transfer parameter  $\Delta Q^{Ag}(x \cong 1)$  was found to be about  $0.3e$ . The corresponding absorption edge is plotted in Fig. 7(a) as a function of  $x$  (solid line). The behavior of the experimental curve (dashed

line) is seen to be in reasonably good agreement. The density of  $d$  states for this charge-transfer parameter at the three alloy concentrations  $x=0.1$ ,  $0.5$ , and  $0.9$  was discussed earlier (Fig. 3). The case of a negative charge-transfer parameter  $\Delta Q^{Ag}(x \cong 1) = -0.2e$  is illustrated in Fig. 7(c). The behavior of the absorption edge for this negative charge transfer is clearly in qualitative disagreement with experiment. This fact supports the arguments presented in Sec. III C which suggest that in Au-Ag the Au atoms must lose electrons to the Ag.

Finally, Fig. 7(d) shows the behavior of the absorption edge for a charge transfer of  $\Delta Q^{Ag}(x \cong 1) = 0.5e$ . The rough estimates of Sec. III C suggest this value to be somewhat larger than is expected physically. For this large charge transfer, the Au  $d$  level is very close ( $0.7$  eV) to the Ag  $d$  level throughout the entire concentration range. It is seen by comparing Fig. 7(d) and the dashed line in Fig. 7(a) that the edge appears at somewhat larger energies for most concentrations than experiment indicates. There is, nevertheless, a rapid drop of the edge near  $x=0$  as the absorption in the alloy changes from being dominated by the Ag to the Au atoms.

Some contributing factors to the remaining disagreement between experiment and theory may be the neglect of  $d$ -band structure, the lack of validity of the linear-charge-transfer assumption [Eqs. (3.4) and (3.5)], or the presence of clustering effects which make the CPA inapplicable. These approximations, discussed earlier, were not expected to affect crucially the qualitative behavior of the optical edge with concentration. The semiquantitative agreement between theory and experiment for a charge transfer from Au to Ag atoms of  $\cong 0.3e$ , which is in good agreement with the theoretical estimates of Sec. III C, is gratifying if somewhat unexpected.

#### ACKNOWLEDGMENTS

We are particularly indebted to R. E. Watson for calling our attention to the importance of the isomer-shift data and for helpful comments. We have also benefited from discussions with B. Velický and R. Jacobs.

\*Supported in part by Grant No. GP-16504 of the National Science Foundation and the Advanced Research Projects Agency.

†Present address: Department of Physics, University of Rochester, Rochester, N. Y.

<sup>1</sup>B. Velický, S. Kirkpatrick, and H. Ehrenreich, Phys. Rev. **175**, 747 (1968).

<sup>2</sup>P. Soven, Phys. Rev. **178**, 1136 (1969).

<sup>3</sup>R. E. Watson, L. Hodges, and H. Ehrenreich (private communication). These calculations may be termed

"quasirelativistic" in the sense that the potentials chosen were relativistic but the (nonrelativistic) Schrödinger equation was solved.

<sup>4</sup>P. R. Wessel, Phys. Rev. **132**, 2026 (1963).

<sup>5</sup>J. Rivory, Opt. Commun. **1**, 53 (1969). An  $x$  dependence similar to that used in the present paper for the first interband optical-absorption edge was found using reflectance and transmittance measurements on thin alloy films.

<sup>6</sup>N. F. Mott, Proc. Cambridge Phil. Soc. **32**, 281

(1936).

<sup>7</sup>L. D. Roberts, R. Becker, F. E. Obenshain, and J. O. Thompson, Phys. Rev. 137, 895 (1965); L. D. Roberts, D. O. Patterson, J. O. Thompson, and R. P. Levey, *ibid.* 179, 656 (1969).

<sup>8</sup>R. E. Watson, H. Ehrenreich, and L. Hodges, Phys. Rev. Letters 24, 229 (1970).

<sup>9</sup>K. Huang, Proc. Phys. Soc. (London) 60, 161 (1966).

<sup>10</sup>E. A. Stern, Phys. Rev. 153, 673 (1967). The concept of charging introduced by Stern refers to differences in  $d$ -wave-function amplitude on each of the two alloy component sites. This should be contrasted to the notion of  $s$  charge transfer discussed here which represents a net charging effect due to  $s$  electrons only. Although there is a small  $d$  component of the wave function which may contribute to charge-transfer effects, it is neglected here.

<sup>11</sup>P. O. Nilsson, Physik Kondensierten Materie 11, 1 (1970). Results of photoemission and optical measurements are presented here.

<sup>12</sup>A more detailed version of these calculations can be found in K. Levin, Ph. D. thesis (Harvard University, 1970) (unpublished).

<sup>13</sup>V. Heine, Phys. Rev. 153, 673 (1967).

<sup>14</sup>J. Hubbard, Proc. Phys. Soc. (London) 92, 921 (1967).

<sup>15</sup>D. Beaglehole and E. Erlbach, Solid State Commun. 8, 255 (1970).

<sup>16</sup>P. W. Anderson, Phys. Rev. 124, 41 (1961).

<sup>17</sup>L. Hodges and H. Ehrenreich, Phys. Letters 16, 203 (1965); L. Hodges, H. Ehrenreich, and N. D. Lang, Phys. Rev. 152, 505 (1966).

<sup>18</sup>F. M. Mueller, Phys. Rev. 153, 659 (1967).

<sup>19</sup>The results of this discussion are applicable to systems with anisotropic Fermi surfaces. Each direction in  $k$  space must be treated separately in this case. If the unhybridized  $s$  band is bounded above and below, then, by the same arguments, there will be a gap in the

hybridized band density of states which contains  $\epsilon_d$ .

<sup>20</sup>An independent relativistic calculation of the band structure of Au has been performed recently by N. E. Christensen and B. O. Seraphin (unpublished). The results used here correspond to Ref. 3.

<sup>21</sup>D. E. Eastman and J. K. Cashion, Phys. Rev. Letters 24, 310 (1970).

<sup>22</sup>The agreement between band-structure calculations and renormalized atom theory has not yet been explored for Au since there appear to be no reliable atomic relativistic calculations.

<sup>23</sup>N. F. Mott, Proc. Phys. Soc. (London) 49, 258 (1937).

<sup>24</sup>Such discrepancies between observed bandwidths and those calculated from hybridization alone were noted by P. W. Anderson, in *Proceedings of the International School of Physics "Enrico Fermi"* (Academic, New York, 1967).

<sup>25</sup>The linear dependence of  $\gamma$  on  $\epsilon_d$  was shown to hold for parabolic  $s$  bands only. This linear dependence, however, seems qualitatively correct, in general, and is assumed to hold for the present model  $s$  band as well.

<sup>26</sup>A. Linde, Ann. Physik 15, 239 (1932).

<sup>27</sup>Equation (3.10) indicates that scattering due to charged impurity effects is the same in both dilute alloys. The additional scattering mechanism which contributes to the resistivity arises from the difference in positions of the bottom of the  $s$  bands in Au and Ag. This mechanism has been treated (see Ref. 8) and its contribution shown to be equal for dilute Au in Ag and dilute Ag in Au. These two theoretical results explain the observed symmetry in the resistivity of  $Au_xAg_{1-x}$  as a function of concentration for  $x$  near 1 and 0.

<sup>28</sup>W. S. Corak, M. P. Garfunkel, C. B. Satterthwaite, and A. Wexler, Phys. Rev. 98, 1699 (1955).

<sup>29</sup>E. Erlbach and D. Beaglehole, Bull. Am. Phys. Soc. 14, 3122 (1969).